PALEOBIOLOGY
A PUBLICATION OF THE · Paleontological SOCIETY

Article

Combined paleohistological and isotopic inferences of thermometabolism in extinct Neosuchia, using *Goniopholis* and *Dyrosaurus* (Pseudosuchia: Crocodylomorpha) as case studies

Mathieu G. Faure-Brac* [ORCID], *Romain Amiot, Christian de Muizon, Jorge Cubo, and Christophe Lécuyer*

Abstract.—The evolution of thermometabolism in pseudosuchians (Late Triassic to the present) remains a partly unsolved issue: extant taxa (crocodilians) are ectothermic, but the clade was inferred ancestrally endothermic. Here we inferred the thermometabolic regime of two neosuchian groups, Goniopholididae (Early Jurassic to Late Cretaceous) and Dyrosauridae (middle Cretaceous to late Eocene), close relatives of extant crocodilians, in order to elucidate the evolutionary pattern across Metasuchia (Early Jurassic to the present), a clade comprising Neosuchia (Early Jurassic to the present) and Notosuchia (Middle Jurassic until the late Miocene). We propose a new integrative approach combining geochemical analyses to infer body temperature from the stable oxygen isotope composition of tooth phosphate and paleohistology and phylogenetic comparative methods to infer resting metabolic rates and red blood cell dimensions. †*Dyrosaurus* and †*Goniopholis* share with extant crocodilians similar lifestyles, body forms, bone tissue organization, body temperatures, metabolic rates, and red blood cell dimensions. Consistently, we infer ectothermy for †*Dyrosaurus* and †*Goniopholis* with the parsimonious implication of neosuchians and metasuchians being primitively ectothermic.

Mathieu G. Faure-Brac and Jorge Cubo. Sorbonne Université, Muséum national d'Histoire naturelle, CNRS, Centre de Recherche en Paléontologie–Paris (CR2P, UMR 7207), 4 place Jussieu, 75005 Paris, France. E-mail: faurebrac.mathieu@gmail.com, jorge.cubo_garcia@sorbonne-universite.fr

Romain Amiot and Christophe Lécuyer. École normale supérieure de Lyon, CNRS, Université Claude Bernard Lyon 1, Laboratoire de Géologie de Lyon–Terre, Planète, Environnement (LGL-TPE),Campus de la Doua, bâtiment Géode, 2, rue Raphaël Dubois, 69622 Villeurbanne Cedex Villeurbanne, France. E-mail: romain.amiot@univ-lyon1.fr, christophe.lecuyer@univ-lyon1.fr

Christian de Muizon. Muséum national d'Histoire naturelle, Sorbonne Université, CNRS, Centre de Recherche en Paléontologie–Paris (CR2P, UMR 7207), 8 rue Buffon, CP 38, Paris, France. E-mail: christian.jourdain-de-muizon@mnhn.fr

Introduction

Thermometabolism is a key feature in the evolution of vertebrates. Two thermogenetic regimes have been identified: endothermy and ectothermy. The first regime involves the production of metabolic heat through nonshivering thermogenesis (Clarke and Pörtner 2010; Rowland et al. 2015), whereas in the second regime, the heat is mainly captured from the environment by behavioral adjustments (Clarke and Pörtner 2010; Rowland et al. 2015). Endotherms have a more elevated body temperature and a higher metabolic rate (i.e., the rate of oxygen consumption measured in $ml(O_2)\ h^{-1}$) than ectotherms (Clarke and Pörtner 2010).

The origin of mammalian and avian endothermy (the only extant endothermic vertebrates) is a central question in evolutionary biology, because higher metabolic rates allow an extension of potential ecological niches, a higher growth rate, and better stamina for active behaviors (McNab 1978; Bennett and

CrossMark

Ruben 1979; Walter and Seebacher 2009). Its presence in both non-avian dinosaurs and non-mammalian synapsids has been extensively investigated using many proxies (e.g., de Ricqlès 1974; Ruben 1995; Amiot et al. 2006; Cubo et al. 2012; Ruben et al. 2012; Legendre et al. 2016; Rey et al. 2017). However, in recent years, another group has been drawing the attention of paleobiologists: Pseudosuchia. Seymour et al. (2004) analyzed the pulmonary and cardiovascular systems of extant crocodilians and suggested that archosaurs were ancestrally/primitively endothermic endotherms. These features include the crocodilian four-chambered heart (Seymour et al. 2004) and the complex arrangement of pulmonary bronchia (Seymour et al. 2004; Farmer and Sanders 2010; Sanders and Farmer 2012; Farmer 2015), similar to those observed in birds. Farmer and Sanders (2010) showed that, more than the general anatomy of the pulmonary system, birds and crocodiles share a unidirectional air flow during respiration, a feature allowing birds to achieve high metabolic rates.

However, despite all these features, crocodilians (as ectotherms) do not display a high metabolic rate (Seymour et al. 2013). Seymour et al. (2004) suggested that the presence of these features in crocodilians is a legacy from their archosaurian endothermic ancestor. It would be congruent with other particularities, such as the presence of fibrolamellar bone (Padian et al. 2004; Tumarkin-Deratzian 2007) and the fast evolution of their mitochondrial genome (Janke and Arnason 1997; Janke et al. 2001), potentially related to high metabolic rate (Seymour et al. 2004).

Using quantitative bone histology, Legendre et al. (2016) concluded that the last common ancestor of all archosaurs possessed a high metabolic rate and was endothermic. Therefore, one can ask when (both temporally and phylogenetically) pseudosuchians lost their endothermy. Seymour et al. (2004) proposed a reversion sometime during the Jurassic (201–145 Ma), concomitant with the spread of ambush-type predation and semiaquatic lifestyle of numerous crocodylomorphs, features strongly associated with the particularities of extant crocodilians' cardiovascular systems. While Legendre et al. (2016) concluded that archosaurs were ancestrally

endothermic, their sample did not allow testing Seymour et al.'s (2004) hypothesis about a reversion to ectothermy in crocodylomorphs.

Legendre et al. (2016) included aetosaurs and rauisuchians in their sample, and their results suggest that all non-crocodylomorph pseudosuchians were endothermic. Since then, new studies brought more data to this subject. Hence, Séon et al. (2020) used isotopic geochemistry to infer the body temperature (T_b) of thalattosuchians. They inferred ectothermy in Teleosauridae, and a more complex picture in Metriorhynchidae, interpreted as being heterothermic endotherms. Moreover, using quantitative histology, Cubo et al. (2020) suggested a common ectothermic ancestor for all notosuchians. Thus, assuming that archosaurs are primitively endotherms, these findings raise two parsimonious possibilities: either a single reversion to ectothermy at the node Crocodylomorpha (or before), and then a reoccurrence of endothermy in metriorhynchids, or converging losses of endothermy in Teleosauridae, Notosuchia, and Eusuchia. Therefore, the thermometabolic status of Metasuchia must be elucidated. While we are aware of the status of extant ectothermic crocodilians and notosuchians, neither Goniopholididae nor Dyrosauridae has been analyzed to date. The aim of this study is to infer the thermometabolic condition of both groups using for the first time two independent proxies in an integrative approach: bone paleohistology and stable isotope geochemistry. Different proxies have been proposed to infer the thermometabolism of extinct species. Some authors looked for the presence of morphological features, such as fur or feathers and respiratory turbinates, as indicators of the presence of homeothermy, which is strongly associated with endothermy (e.g., Ruben 1995; Ji et al. 2006; Ruben et al. 2012; Zhou et al. 2013). However, these features are only indirectly linked to endothermy, and the potential causal links are still being debated. Other studies proposed the modeling of the thermic exchange with the environment based on the 3D reconstruction of extinct organisms (e.g., Florides et al. 2001). Another possibility is the study of cardiovascular physiology, as several parameters are associated with the metabolic rate (for a review, see

Seymour 2013, 2016). Bone histology was extensively used in this area, both qualitatively and quantitatively, for its strong connection with metabolic rate (e.g., de Ricqlès 1974; Padian et al. 2004; Montes et al. 2007; Olivier et al. 2017; Fleischle et al. 2018; Cubo and Jalil 2019; Faure-Brac and Cubo 2020). Finally, stable isotope geochemistry was extensively used to infer the body temperature of extinct species (Amiot et al. 2006; Bernard et al. 2010; Rey et al. 2017; Séon et al. 2020).

Bone Histology

Amprino (1947) proposed that the structure of bone tissue records the bone growth rate (BGR). This finding was corroborated by Montes et al. (2010) in a phylogenetic context. In parallel, a link between BGR and resting metabolic rate (RMR, a standardized metabolic rate taking account of the effect of body mass) was shown by Montes et al. (2007). It is worth noting that the first relationship had been tested experimentally (Starck and Chinsamy 2002), whereas the relationship between RMR and BGR is correlational. A test of a causal relationship is lacking. Although correlational, we can use the quoted relationship to infer the RMR of extinct species using bone structure in phylogenetic comparative approaches.

Two mechanisms of osteogenesis that produce different bone structures have been described. The first, static osteogenesis (SO), is related to high BGR. SO quickly produces highly vascularized bone tissues composed of woven bone (isotropic fibers) and globular osteocyte lacunae displaying radiating canaliculi (Marotti 2010; Prondvai et al. 2014; Stein and Prondvai 2014; Cubo et al. 2017). The second, dynamic osteogenesis (DO), is associated with low BGR. DO produces nearly to completely avascular bones composed of parallel fibered bone that appears either as anisotropic tissue containing elongated lacunae when fibers run perpendicular to the direction of transmission of cross-polarized light or as isotropic and containing pinhead-shaped lacunae when fibers run parallel to the direction of transmission of cross-polarized light (Marotti 2010; Prondvai et al. 2014; Stein and Prondvai 2014; Cubo et al. 2017). To sustain rapid growth, SO requires higher amounts of energy

than does DO, that is, a higher metabolic rate (Montes et al. 2007). However, identifying SO structures is not a sufficient criterion to suggest an endothermic condition, as exceptions occur, notably in extant crocodilians (Padian et al. 2004; Tumarkin-Deratzian 2007).

As an alternative, Legendre et al. (2016) proposed to use a phylogenetic comparative method, phylogenetic eigenvector maps (PEM; Guénard et al. 2013) to infer RMR values for extinct species using histological variables and phylogenetic relationships of a sample of extant vertebrates as explanatory variables. This method of quantitative histology was extensively used in various groups of vertebrates and provided promising results (Legendre et al. 2016; Olivier et al. 2017; Fleischle et al. 2018; Cubo and Jalil 2019; Cubo et al. 2020; Faure-Brac and Cubo 2020). As endothermy necessitates high RMR to fuel heat production, inferring the latter seems an appropriate proxy to infer the thermometabolic regime of extinct taxa.

Recently, another approach using quantitative histology was proposed by Huttenlocker and Farmer (2017). They showed a high correlation between red blood cell (RBC) width (RBC_w) and area (RBC_a) with the size of the bone vascular cavities. This finding is consistent with the observation that the smallest RBCs are found in vertebrates with the highest energetic expenditure, that is, the highest metabolic rate (mammals and birds). Indeed, smaller RBCs are associated with faster O_2 kinetic uptake (Holland and Forster 1966), allowing higher metabolic rates. Huttenlocker and Farmer (2017) were able to infer RBC width and area for extinct species using quantitative histology, and their methodology was then applied by Cubo et al. (2020), using PEM, with success. The combined use of these proxies is valuable, as they produce independent inferences for the same variable, thermometabolism.

Isotopic Geochemistry: Basic Principles

Relationships between Vertebrate Body Water, Diet Water, and Ambient Water.—The oxygen isotope composition of phosphate in vertebrate apatite ($\delta^{18}O_p$) depends on both the mineralization temperature of the skeleton and the oxygen
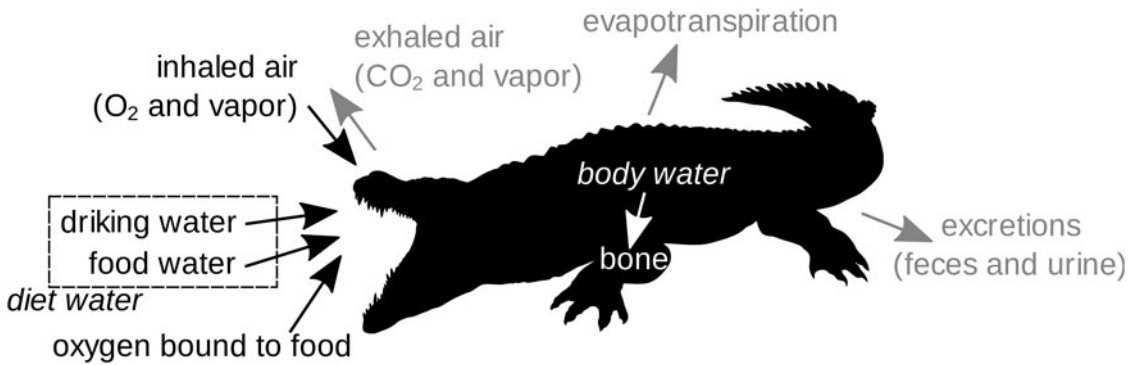
FIGURE 1. Diagram summarizing the inputs (black arrows) and outputs (gray arrows) of oxygen between a living organism and its environment. The white arrow indicates the fractionation occurring during the mineralization of the bones. From ambient water (gathering all possible sources of water, see text), the oxygen is incorporated into the drinking water and the solid food (with both water and oxygen bound to it). Both of these sources constitute the diet water that is incorporated in the body water. The drinking water is itself from the different sources of ambient waters. The crocodilian shape used was obtained on phylopic.org.

isotope composition of its body water ($\delta^{18}O_{bw}$) (Kolodny et al. 1983; Longinelli 1984; Luz et al. 1984). For all vertebrates, the $\delta^{18}O_{bw}$ value depends on the oxygen isotope composition of diet water ($\delta^{18}O_{dw}$), which mainly includes drinking water and water-bearing solid food (e.g., leaves, herbs, roots, meat). The oxygen isotope composition of diet water is itself directly related to the oxygen isotope composition of ambient water ($\delta^{18}O_{aw}$); which means freshwater (river, lake) or seawater ($\delta^{18}O_{sw}$) for aquatic vertebrates and meteoric waters ($\delta^{18}O_{mw}$) for terrestrial vertebrates (Luz et al. 1984; D'Angela and Longinelli 1990; Kohn 1996; Langlois et al. 2003). Aquatic vertebrates such as fish have $\delta^{18}O_{bw}$ values similar to those of the water masses where they live. In the case of semiaquatic vertebrates, $\delta^{18}O_{bw}$ values are influenced by their aquatic environments but also by a combination of input and output oxygen fluxes. Input oxygen fluxes to the animal body are air through the lungs and associated water vapor, food, and drinking water. Output oxygen fluxes from the animal body are feces and urinary water, urea or uric acid, transcutaneous and exhaled water vapor (via respiration or, for some mammals like carnivores, via panting), and expired carbon dioxide (Fig. 1).

Considering the oxygen isotope fractionation that takes place during evapotranspiration (evaporation of body water) and the combustion of food by atmospheric oxygen that has a $\delta^{18}O$ value much higher (+23‰) than those of other reservoirs ($-3‰ < \delta^{18}O_{sw} < +2‰$; $-30‰ < \delta^{18}O_{mw} < +2‰$), $\delta^{18}O_{bw}$ values commonly increase by a value between 0 and +2‰ for most known semiaquatic and air-breathing vertebrates (Barrick et al. 1999; Amiot et al. 2007). Such heavy oxygen isotope enrichment of the body water relative to the diet water may reach up to +6‰ for terrestrial vertebrates (Longinelli 1984; Wolf et al. 2013).

Relationships between Vertebrate Body Temperature and Ambient Water.—In the framework of this study, the calculation of crocodylomorph body temperature is performed according to the following protocol and assumptions:

- The enrichment in heavy oxygen isotope (^{18}O relative to ^{16}O) of crocodylomorph body water relative to ambient water does not exceed +2‰ (Amiot et al. 2007).
- The generic equation, which relates the $\delta^{18}O_P$ to mineralization temperature T and $\delta^{18}O_w$, is expressed as follows according to Kolodny et al. (1983) as modified by Lécuyer et al. (2013):

$$T = 117.4 - 4.5(\delta^{18}O_p - \delta^{18}O_{aw}) \quad (1)$$

becoming equation (2)

$$T = 117.4 - 4.5(\delta^{18}O_p - \delta^{18}O_{bw}) \quad (2)$$

when transposed to the case of aquatic or semiaquatic vertebrates.

- The use of isotopic fractionation equations that relate $\delta^{18}O_p$ to $\delta^{18}O_{aw}$ in the case of extant mammals, theropods, and turtles.

  o For mammals (Amiot et al., 2004):

$$\delta^{18}O_{aw} = 1.1128 \times \left(\delta^{18}O_p - 26.41\right) \quad (3)$$

  o For theropods (Amiot et al., 2015):

$$\delta^{18}O_{aw} = 1.119 \times \left(\delta^{18}O_p - 24.222\right) \quad (4)$$

  o For turtles (Barrick et al. 1999, modified by Pouech et al. 2014):

$$\delta^{18}O_{aw} = 0.994 \times \left(\delta^{18}O_p - 21.197\right) \quad (5)$$

- The oxygen isotope composition of ambient water $\delta^{18}O_{aw}$ (mainly derived from meteoric waters) is estimated by using fractionation equations applied to theropods, mammals, or turtles co-occurring with studied dyrosaurids and †*Goniopholis*.
- Finally, equation (2) is solved for body temperature, T_b, by using previously calculated $\delta^{18}O_{aw}$ (equations 3–5) with the addition of body water ^{18}O-enrichment to obtain $\delta^{18}O_{bw}$ and measured $\delta^{18}O_p$ of Dyrosauridae and †*Gonophiolis*.

Graphic Representation of Calculations and Data for Discussion of the Thermophysiological Status.—Calculations and data are finally highlighted by using a $\delta^{18}O_p$–$\delta^{18}O_{aw}$ bivariate plot that discriminates between the fields of ectothermic–poikilothermic and endothermic–homeothermic vertebrate taxa. Those fields are constructed on the basis of a nomogram that represents body isotherm values. If tested dyrosaurids and †*Goniopholis* had ecto-poikilothermic thermophysiologies including behavioral thermoregulation similar to those of extant crocodilians, their T_b values would fall within a preferred range of 26°C–36°C (Markwick 1998). If they were endotherms, then their body temperature would most likely fall within the 36°C–40°C range, as in most modern endotherms. Thus, the distribution of data in the predefined fields of body temperatures will offer a basis for

discussing the thermophysiological status of vertebrate taxa studied.

To infer the thermometabolic condition of Goniopholididae and Dyrosauridae, both bone histology and isotopic geochemistry were used. We describe the bone cross sections of two specimens of these groups and use them to infer RMR, RBC_w, and RBC_a using quantitative histology. We use already published isotopic data for Goniopholididae and present here new isotopic data for Dyrosauridae, with the aim of estimating their T_b. Finally, we propose a putative state of their thermometabolism using all these parameters. The null hypothesis is that they were ectothermic organisms because of their phylogenetic proximity and ecological similarity with extant crocodilians.

Materials and Methods

Material

Quantitative Histology.—Two extinct species were studied: †*Goniopholis simus* Owen, 1879 from the Berriasian (Early Cretaceous) of Cherves-de-Cognac, France (Muséum national d'Histoire naturelle/Paris Museum of Natural History: MNHN CHE.02.046) and †*Dyrosaurus* sp. Pomel, 1894 from the Ypresian (Eocene) of North Africa. For all species, both extinct and extant, we studied the femur.

Their data were incorporated into two datasets comprising histological variables and the variables of interest (RMR or RBC width/area) of a set of extant species. Both datasets are from Cubo et al. (2020). The first one, used in RMR inferences, comprises 18 extant species. The second one, used in RBC inferences, comprises 14 extant species. The complete list of included species is given in the Supplementary Material and Methods.

Isotopic Geochemistry.—Depending on the amount of available material, we sampled enamel or a mixture of enamel–dentine of several teeth coming from Paleocene dyrosaurid crocodylomorphs, from the pantodont eutherian †*Alcidedorbignya inopinata* de Muizon & Marshall, 1992, both provided by C. de Muizon, and a shell bony plate from the Podocnemidid turtle †*Roxochelys* sp. Price, 1953 recovered from the paleontological site of Tiupampa (Bolivia).

The details of the samples are given in Supplementary Table 1.

Geochemical data of †*Goniopholis* sp. and its associated fauna from the Berriasian site of Cherves-de-Cognac (France) were already published by Pouech et al. (2014). A selection of relevant values including mammals, turtles and theropod dinosaurs was then reanalyzed in terms of †*Goniopholis* T_b.

Methods

Preparations of Sections.—Thin sections of †*Goniopholis simus* and †*Dyrosaurus* sp. were prepared at the closest possible level to the middle of the diaphysis. For each species, one cross section from the mid-shaft of a femur was prepared and consequently analyzed. They were mounted on a glass slide following the method described in Lamm (2013). These sections were deposited at the vertebrate hard tissues histological collection of the MNHN, where they are available upon request to the curator, with the respective access numbers MNHN-F-Histos-2751 (†*Goniopholis*) and MNHN-F-Histos-2752 (†*Dyrosaurus*). The histological terminology follows Francillon-Vieillot et al. (1990) with addenda and revision from Prondvai et al. (2014).

Cross sections were observed under a Nikon Eclipse E600 POL microscope, either in linearly polarized light (LPL) or in cross-polarized light (XPL) with a lambda wave plate, in order to determine the nature of bone tissue in each topologic region using patterns of isotropy/anisotropy (Bromage et al. 2003; Faure-Brac et al. 2019). Variations in isotropy allowed us to assess orientation and organization of collagen fibers. Anisotropic fibers, which appear blue/yellow under XPL with a lambda compensator, are highly organized and parallel thus and perpendicular to the direction of propagation of XPL. For isotropic fibers, which appear red under XPL with a lambda compensator, two possibilities exist: either fibers lie in parallel and are parallel to the direction of propagation of XPL (i.e., cut transversally) or woven bone (for a review, see Faure-Brac et al. 2019).

Histological Variables.—Pictures were taken at different magnifications and analyzed with the software ImageJ v. 1.8.0_172 (Rasband 1997) to quantify the different histological variables. Three were quantified: relative primary osteon area (RPOA) for RMR inferences (described as primary osteon density by Fleischle et al. 2018) and harmonic mean caliber (HMC) and minimal caliber (can$_{min}$) of vascular cavities for inferences of RBC width/area (Huttenlocker and Farmer 2017).

RPOA was quantified as described by Fleischle et al. (2018): an area is delimited in the deepest primary cortex, and the surface occupied by primary osteons is quantified (see Fig. 2A). To quantify this variable in the deep, primary cortex is necessary, because our sample of extant animals only contains juveniles: therefore, in extinct adult taxa, we have to analyze the bone tissue placed as close as possible to their initial growth stage. RPOA corresponds to the ratio between the quoted variables:

$$RPOA = S_{osteon}/S_{total} \qquad (6)$$

where S_{osteon} is the surface occupied by primary osteons, and S_{total} is the surface of the studied area. If some secondary bone is present in the total area, its surface is deducted from the S_{total} before the calculation of RPOA.

HMC and can$_{min}$ of vascular canals were quantified in the outer cortex, as our sample of extant animals is composed of adults only. In accordance with Huttenlocker and Farmer (2017), up to fifty canals were quantified in each section (see Fig. 2B). We delineated canals and fit the largest ellipse in them. Then, we measured the minimal axis. HMC was calculated using the following equation:

$$HMC = \frac{n}{\sum_{i=1}^{n}(1/x_i)} \qquad (7)$$

where n is the number of measured vascular cavities, and x_i the value of the minimal axis for the ith cavity. can$_{min}$ is simply the smallest minimal axis in our sample. The dataset of extant species used to infer RMR is from Cubo et al. (2020), and the dataset used to infer RBC variables is from Huttenlocker and Farmer (2017). All values for the extinct species were quantified in this study.

Phylogeny.—Two phylogenies were used, one for each set of taxa. The phylogeny used to infer RMR is an amended tree taken from Cubo et al. (2020), and the one used to infer
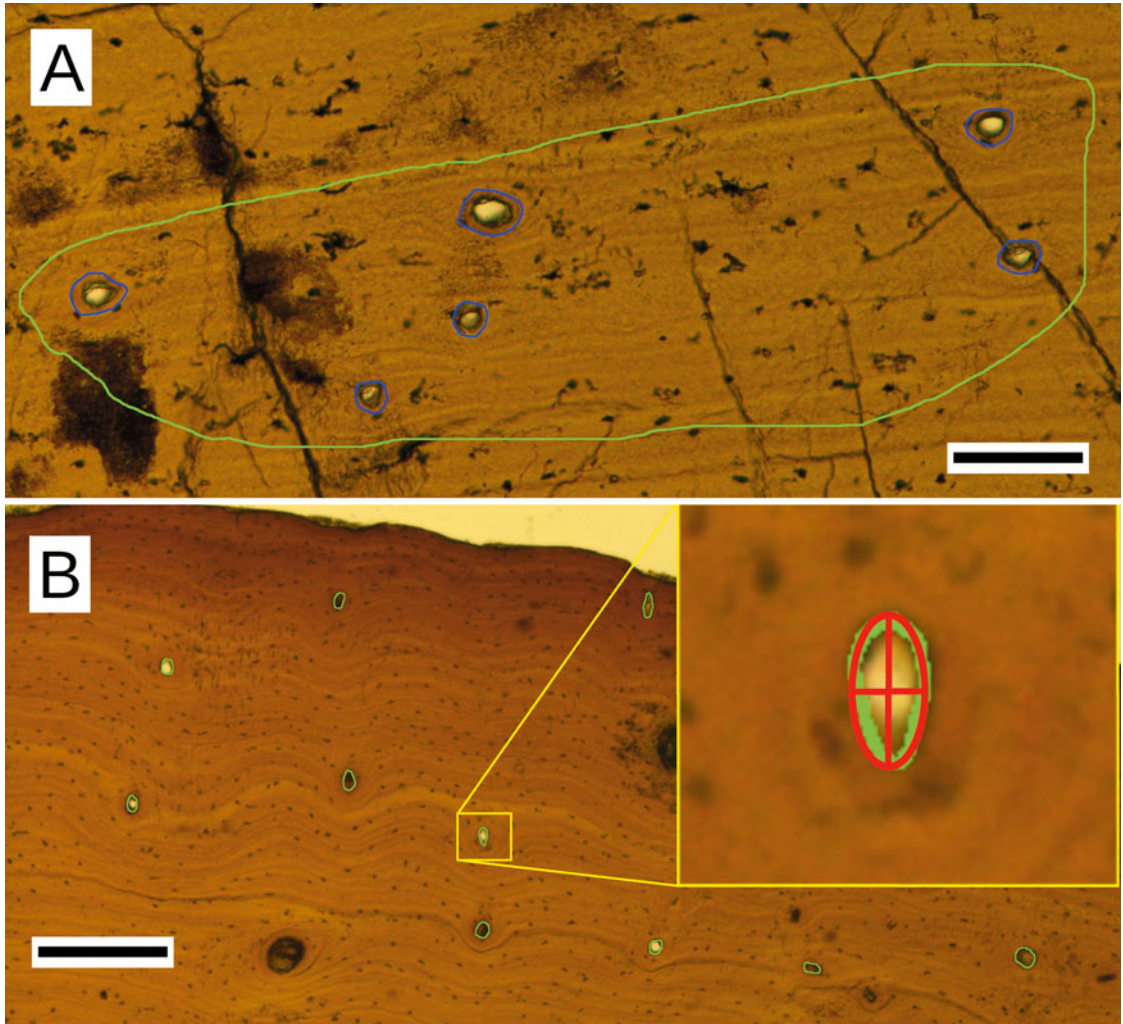
FIGURE 2. Example of the quantification of variables in the histological section of †*Goniopholis simus*. A, Inner layer, close to the medulla. The area of the green circle constitutes the S_{total} of the relative primary osteon area (RPOA), and the S_{osteon} is the sum of all areas of the blue circles (equation 6). B, Outer layer. The green circles identify the vascular canals. As shown in the zoomed part, an ellipse is fit by the software in the circle, and the minimal axis is used in the harmonic mean caliber (HMC) computation (equation 7). Scale bars, 100 µm.

RBC variables is amended from Huttenlocker and Farmer (2017). In both cases, extinct species were removed and replaced with †*Dyrosaurus* sp. and †*Goniopholis simus*. Their placement follows the consensual phylogeny presented by Puértolas-Pascual et al. (2020). As the phylogenetic comparative method necessitates branch lengths, we dated the trees using the minimal age of apparition of each node. Branch lengths reflect, then, the time between the apparition of two successive nodes, or between a node and a leaf. Age of a given node was

computed as the minimal age of the oldest fossil included in it and was taken from the Paleobiology Database (https://paleobiodb.org, last accessed 28 June 2020).

Phylogenetic Eigenvector Maps.—A summary of the principal steps of the protocol is presented here. The full protocol is available in Guénard et al. (2013) and in the Supplementary Material and Methods. PEM operates in two steps: (1) the construction of predictive models and the selection of the better performing one and (2) the inference of extinct species' values.

For each of the three analyses, a model is chosen among a set of models comprising (1) a model including the phylogeny and the values of the studied variable of extant species and (2) many models comprising the phylogeny, the values of the studied variable of extant species, and one histological variable. After the choice of the model through the use of a corrected Akaike's information criteria (AICc), inferences of RMR values and RBC dimensions for extinct species are computed. We used the package MPSEM (Guénard et al. 2013), with the software R v. 3.5.1 (R Development Core Team 2008). The script, data, and phylogenies used are given in the Supplementary Files.

Isotopic Geochemistry.—Chemical preparation and measure of the oxygen isotope composition of tooth and bone apatite phosphate were realized following the protocol published in Lécuyer et al. (1993) and detailed in the Supplementary Material and Methods. Phosphate from tooth enamel and bone was isolated in the form of silver phosphate crystals that were pyrolyzed at 1450°C using an elemental analyzer and then analyzed with an isotopic ratio mass spectrometer.

The measurements were calibrated by performing a two-point calibration using the international reference materials NBS120c ($\delta^{18}O_{VSMOW}$ = 21.7‰; Lécuyer et al. 1993) and NBS127 (BaSO$_4$, $\delta^{18}O_{VSMOW}$ = 9.34‰; Gonfiantini et al. 1995). Isotopic compositions are quoted in the standard δ notation relative to VSMOW. Silver phosphate precipitated from standard NBS120c (natural Miocene phosphorite from Florida) was repeatedly analyzed ($\delta^{18}O$ = 21.76 ± 0.12‰; n = 20) along with the silver phosphate samples derived from the vertebrate remains. Chemical extraction, analyses, and measurements were performed at the Laboratoire de Géologie de Lyon–Terre, Planète, Environnement.

Results

Histological Description

†*Goniopholis simus.*—The bone is partly fractured and invaded by fungi, making observations difficult to interpret in some places, especially in the posterior and dorsal areas (Fig. 3A). Fractured regions are not problematic: borders coincide most of the time, suggesting only a displacement of limited parts of the bone without loss of material. Regions invaded by fungi are especially problematic, as the fungi hide histological features of interest, such as the fibers' organization. The majority of the section, however, displays a good preservation, allowing us to infer an interpretation of the paleobiology of †*Goniopholis*.

The section is nearly circular, displaying a large medullary cavity, free of spongious bone. The bone is slightly thicker in posterodorsal areas, leading to a slightly off-center medulla (Fig. 3A). We observed a poor vascularization, predominantly concentrated in the deep layers of the cortex, associated with primary small-sized primary osteons. The fibers' orientation is predominantly longitudinal (i.e., parallel to the main axis of the bone). The following histological description is based on observation of the anterior region (Fig. 3A, black square, B,E). Osteons appear associated in disorganized bundles in the deep cortex (Fig. 3B, layer A) but form circular rows closer to the periosteum (Fig. 3B, layers C_1–C_4). Except for a small part in the postero-dorsal region exhibiting some remodeling (Fig. 3F), tissue is mostly primary. The specimen is an adult, as suggested by the presence of an avascular outer circumferential layer, or external fundamental system (EFS; Fig. 3B, layer E).

This cross section is composed of alternating layers formed at a high growth rate (containing a scaffold of SO bone and primary osteons infilled with DO bone: layers A and C_1–C_4 in Fig. 3B) and layers of DO bone tissue formed at low growth rate (Fig. 3B, layers B_1–B_4, D, E). The thick layer A is composed of a scaffold of SO bone containing primary osteons (Fig. 3B, layer A). Layers C_1 to C_4 have the same structure but are thinner than layer A (Fig. 3B, layers C_1–to C_4). They are perfectly recognizable by the presence in the scaffold of SO osteocyte lacunae (globular, with radiating canaliculi) (Fig. 3C, black arrows) and isotropic tissue. In strong contrast, layers B_1 to B_4 display DO features (Fig. 3B, layers B_1–B_4), showing alternatively the two types of lacunae and fiber orientation (Fig. 3D, white and gray arrows). It can be explained by a plywood structure, that is, a succession of thin layers of lamellar bone having orthogonal orientations, visible under XPL.
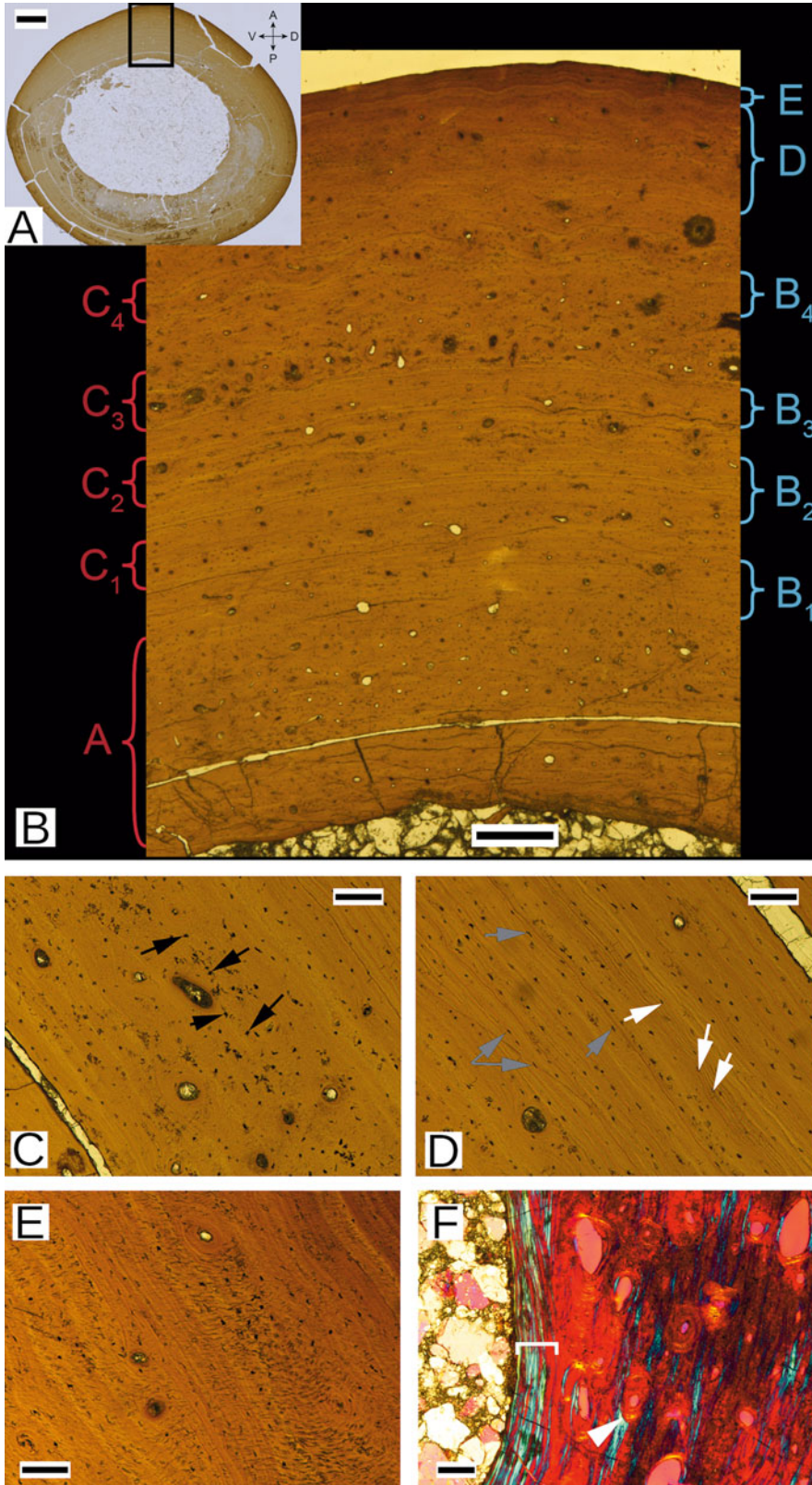
FIGURE 3. Histological section of †*Goniopholis simus*. A, General view of the cross section. The arrows indicate the orientation of the section (A: anterior, P: posterior, V: ventral, D: dorsal). Picture obtained using a Hirox 2000 microscope. B, Details of the anterior region of the section. Red layers are high growth-rate layers and dark blue layers are low growth-rate layers. Layer A: Layer with a bundle organization of osteons. Layers B_1–B_4: Highly organized tissues, poorly organized. Layers C_1–C_4: Layers with circular rows of osteons. Layer D: Layer displaying Sharpey's fibers. Layer E: External fundamental system. C, Focus on a layer with circular rows of osteons. Black arrows indicate typical static osteogenesis (SO) osteocyte lacunae. D, Focus on a highly organized layer. Gray arrows indicate elongate dynamic osteogenesis (DO) osteocyte lacunae, white arrows indicate pinhead DO osteocyte lacunae. E, Focus on the layer displaying Sharpey's fibers. F, Focus on deep cortex displaying secondary bone with the endosteal bone (white bracket) and secondary osteons (white arrowhead). Scale bars: A, 3000 μm; B, 500 μm; C, 200 μm; D–F, 100 μm.

These features suggest a first phase of rapid growth corresponding to the deep cortex (Fig. 3B, layer A). The outer part of the cortex, from the end of the deep cortex to the EFS, displays an alternation of periods of slow BGR (Fig. 3B, layers B_1–B_4), shown by the organized tissues, and periods of faster BGR, shown by the layers of osteons in circular rows (Fig. 3B, layers C_1–C_4). This organization, the lamellar-zonal, is typical of extant crocodilians (Padian et al. 2004; Tumarkin-Deratzian et al. 2007).

In addition to the primary bone, there are two kinds of secondary bone occurrences. The first one is present on the margin of the medullary cavity: endosteal bone. It consists of highly organized bone, completely avascular, exhibiting a strong anisotropy (Fig. 3F, white bracket). The second kind of secondary bone corresponds to the presence of secondary osteons (Fig. 3F, white arrowhead). However, remodeling is scarce, suggesting a young adult.

This pattern of alternating layers of SO and DO bone is observed everywhere in the section and is relatively homogenous, with some notable exceptions. The anterior area displays more bands of high growth rate than other areas, suggesting more active growth than in other areas. It is associated with the presence of Sharpey's fibers, close to the periosteum (Fig. 3B, layer E). These fibers reveal the attachment of a soft tissue, muscles, or ligaments.

†*Goniopholis* presents a bone histology similar to that observed in extant crocodilians, with a lamellar-zonal histological organization. This animal was an adult according to the presence of the EFS but seems to be relatively young, as remodeling is still scarce. According to these features, it probably possessed a metabolic rate similar to that of extant crocodilians. Despite the fractures and fungal degradation, the section displays enough primary bone layers to allow a good quantification of variables and hence for performing the PEM analysis.

†*Dyrosaurus sp.*—The cross section of †*Dyrosaurus* is well preserved (Fig. 4A). There are some fractures, and we can identify invasion by fungi, but they are relatively scarce and do not impact the analysis of the section. The section is also nearly circular with a smaller medullary cavity compared with †*Goniopholis*; it is also free of bone trabeculae. Vascularization is dense but consists essentially of large secondary osteons. Primary osteons are scarce, but still present, and much smaller than the secondary ones. The vascularization is longitudinal in majority, as for †*Goniopholis*. The presence of an EFS suggests that this organism was an adult, and probably aged. Harvesian bone constitutes a large part of the section, and more than 15 lines of arrested growth (LAGs; Fig. 4D, white arrowheads, and visible on Fig. 3B, from layer B1 to E) are present in the outer half of the cortex. Therefore, tissue is essentially secondary in the deep cortex, which means that the recording of the first stages of life has been lost.

We observed two major types of primary bone. On one hand, the great majority of the remnant primary bone is constituted of DO bone: poorly vascularized, if not completely avascular (Fig. 4B, layers B_1–B_5), strongly anisotropic, and associated with elongated osteocyte lacunae (Fig. 4D, white arrows). Contrary to †*Goniopholis*, we cannot easily find an isotropic tissue with pinhead lacunae, suggesting there is no change in the direction of fibers.

On the other hand, we can find thin bands of circular rows of primary osteons as in †*Goniopholis*. These osteons are associated with isotropic fibers and globular lacunae, typical of SO bone (Fig. 4D, black arrows). As a large part of the bone is remodeled, it is difficult to
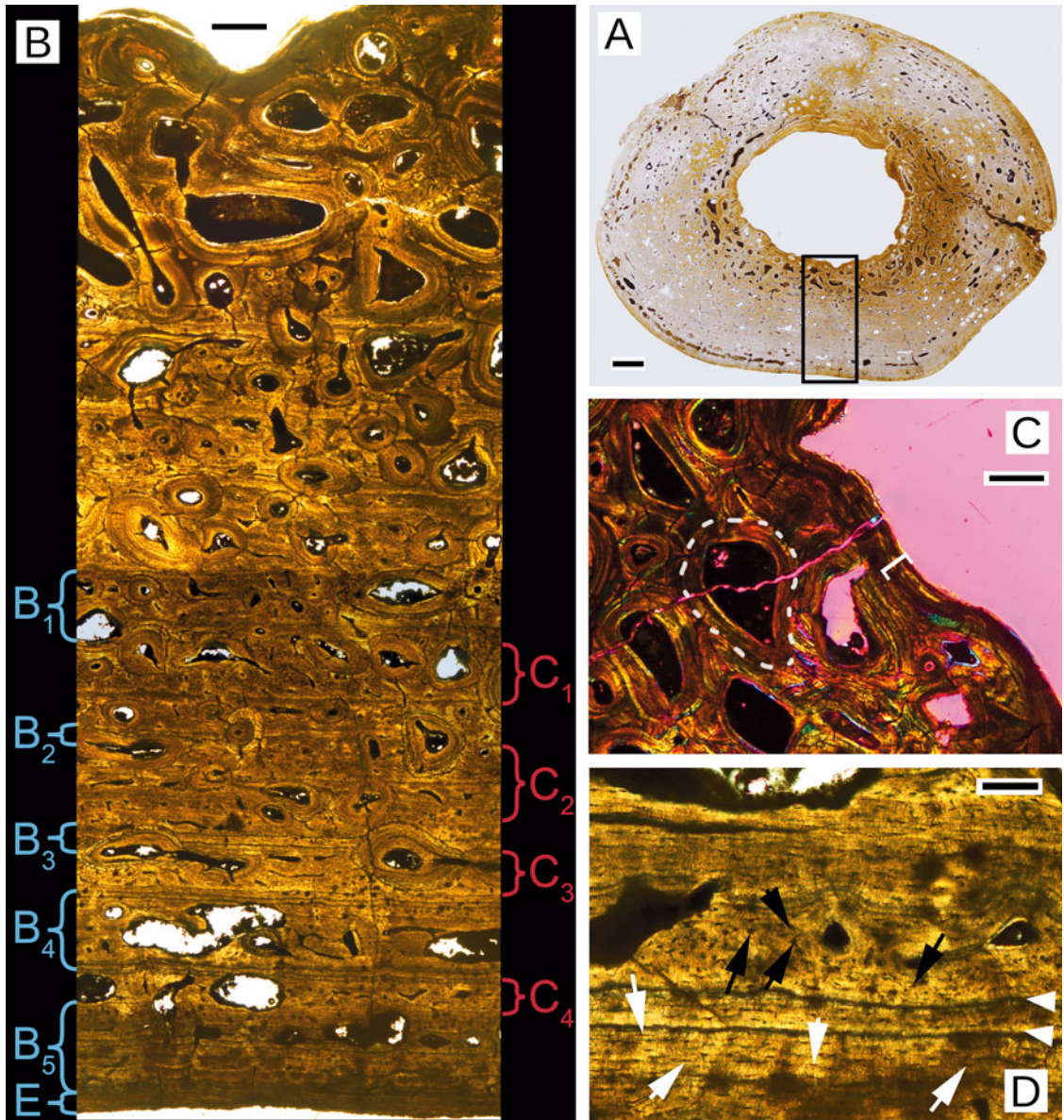
FIGURE 4. Histological section of †*Dyrosaurus* sp. A, General view of the cross section. Picture obtained using a Hirox 2000 microscope. Viewed in natural light. B, Details of a region, with the indication of the different layers of growth rate. Red layers are high growth-rate product, and blue are low growth-rate product. Viewed in linearly polarized light (LPL). C, Focus on the deep cortex, on the margin with the medulla. White bracket indicates the endosteal bone, and white dotted line indicates the limit of a secondary osteon. Viewed in cross-polarized light (XPL). D, Focus on primary bone. Black arrows indicate static osteogenesis (SO) produced osteocyte lacunae, white arrows indicate dynamic osteogenesis (DO) produced osteocyte lacunae. Viewed in LPL. Scale bars: A, 3000 µm; B, 500 µm; C, 200 µm; D, 100 µm.

establish the exact number of these rows. It seems we can find at least four of them (Fig. 4B, layers C_1–C_4). Approaching the EFS, the rows become thinner. Moreover, on the outer half of the cortex, numerous LAGs are present. They are especially abundant and close to

each other near the EFS. These features suggest a continuous growth, but steadily decreasing in magnitude and becoming negligible by the end of the specimen's life.

Secondary bone is particularly present in this section. It consists of endosteal bone (Fig. 4C,

TABLE 1. Results of quantification and phylogenetic eigenvector maps (PEM) inferences for both extinct studied species. n (ost) is the number of quantified osteons, n(can) the number of quantified vascular canals. HMC, harmonic mean caliber; RBC, red blood cell; RMR, resting metabolic rate; RPOA, relative primary osteon area.

Species	Histological variables					RMR (ml(O_2) h^{-1} g$^{-0.67}$)			RBC width (μm)		RBC area (μm^2)	
	n (ost)	RPOA	n (can)	can$_{min}$ (μm)	HMC (μm)	Lower	Center	Upper	Value	Confidence	Value	Confidence
†*Dyrosaurus* sp.	85	0.077	47	14.9	21.5	0.144	0.227	0.358	11.85	± 1.75	165.94	± 25.68
†*Goniopholis simus*	20	0.059	50	10.3	20.5	0.139	0.205	0.305	8.42	± 1.17	132.35	± 18.55

white bracket) and, essentially, haversian bone, characterized by huge secondary osteons (Fig. 4C, delineated by the white dotted line). They are found nearly everywhere in the section, occupying all the space in the deep cortex, gradually decreasing in abundance toward the periphery, and becoming nearly absent near the EFS.

The bone is relatively homogenous, but it is tricky to identify differences in the growth pattern, as the secondary bone invaded a large part of the primary growth, especially the deeper half cortex.

As for †*Goniopholis*, we observed a typical lamellar-zonal bone as currently documented in extant crocodilians. The extension of secondary bone is more problematic than for †*Goniopholis*, but there is still enough primary bone for measuring the required variables and performing PEM inferences.

Quantitative Histology.—The quantified variables were measured using equations (6) and (7) and are presented in Table 1. Extinct taxa display values of RPOA similar to those observed in *Crocodylus* (†*Dyrosaurus*: 0.077; †*Goniopholis*: 0.059; *Crocodylus*: 0.052). The same is found for both can$_{min}$ (†*Dyrosaurus*: 21.5 μm; †*Goniopholis*: 20.5 μm; *Alligator*: 22 μm) and HMC (†*Dyrosaurus*: 14.9 μm; †*Goniopholis*: 10.3 μm; *Alligator*: 13.2 μm).

The AICc and R^2 values for each model and analysis are presented in Table 2. For all analyses, a model including a histological variable was chosen. For both RBC analyses, a model including the can$_{min}$ as explanatory variable was chosen (RBC$_w$, $R^2 = 0.828$, AICc = 49.749; RBC$_a$, $R^2 = 0.981$, AICc = 128.285). It was unquestionably better than others for the RBC$_a$ analysis and was preferred to the model

TABLE 2. Metrics from corrected Akaike's information criteria (AICc) on different models for the different analyses. Bold type indicates the chosen model. can$_{min}$, minimal caliber; HMC, harmonic mean caliber; RBC, red blood cell; RMR, resting metabolic rate; RPOA, relative primary osteon area.

Model	R^2	AICc
Analysis 1: RMR Phylogeny	0.979	29.912
Phylogeny + RPOA	**0.972**	**30.052**
Analysis 2: RBC width Phylogeny	0.733	58.328
Phylogeny + can$_{min}$	**0.828**	**49.749**
Phylogeny + HMC	0.843	54.455
Analysis 3: RBC area Phylogeny	0.976	131.837
Phylogeny + can$_{min}$	**0.981**	**128.285**
Phylogeny + HMC	0.978	130.338

including HMC ($R^2 = 0.843$, AICc = 54.455) because of its better AICc score and similar R^2 coefficients for the RBC$_w$ analysis. However, for RMR analysis, model outputs with and without RPOA were similar. Although the model including the phylogeny exclusively is slightly better from a statistical point of view ($R^2 = 0.979$, AICc = 29.912), we chose to use a model including RPOA as an explanatory variable ($R^2 = 0.972$, AICc = 30.052), as it is more relevant from a biological point of view.

Using these models, we were able to infer values of RMR, RBC$_w$, and RBC$_a$ for both extinct taxa. These values are presented in Table 1 and Figure 5 (see Supplementary Fig. 1 for a version with cross-values). Shapiro-Wilk tests were performed on residuals for all models. A log transformation was necessary for the model using RPOA for RMR inference ($p = 0.0374$ before transformation; $p = 0.8361$ after transformation). We used natural
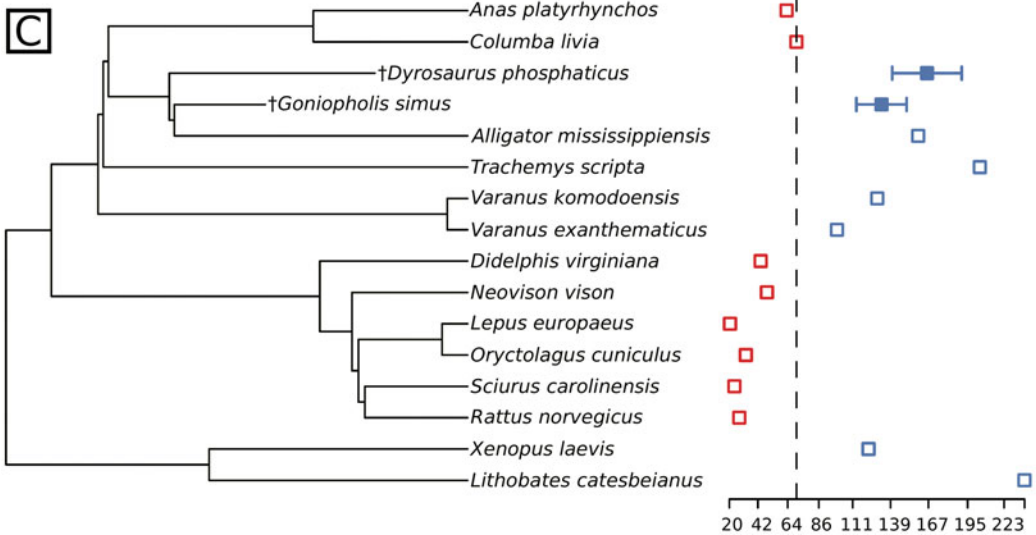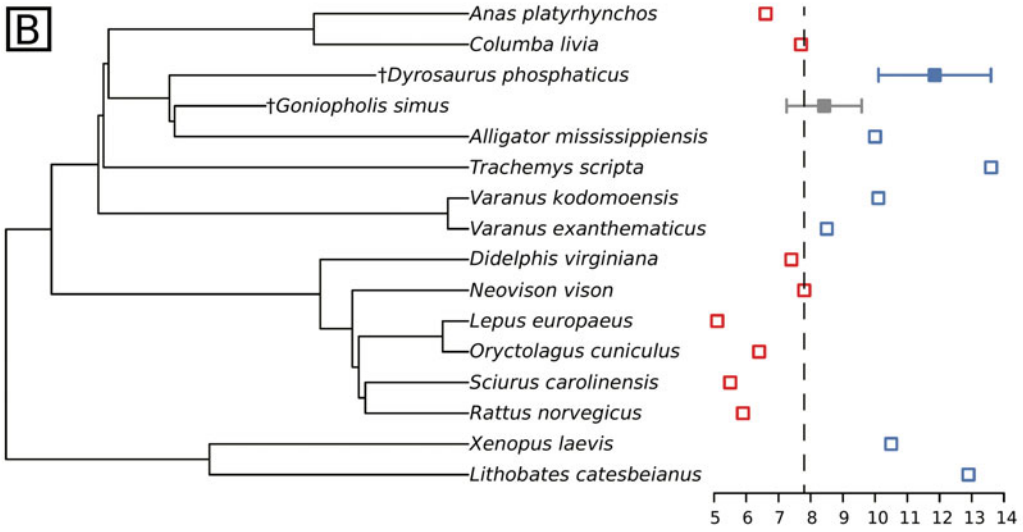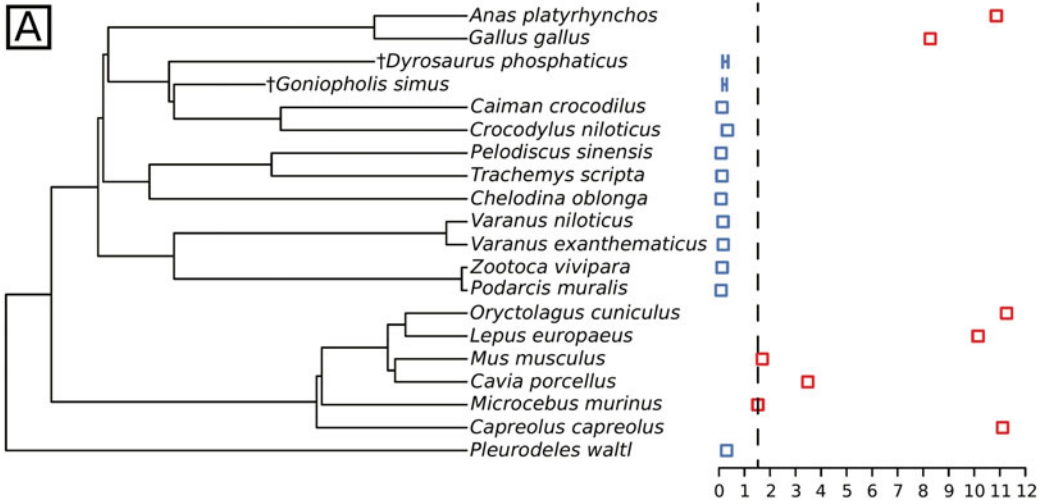
FIGURE 5. Results of the different analyses conduct using phylogenetic eigenvector maps (PEM). Empty squares are empirical data of extant tetrapods. Brackets (with filled square, if present) are inferred data of extinct neosuchians. Red indicates an endotherm, blue an ectotherm, and gray an unknown condition. Dotted line indicates the limit between endothermy and ectothermy, based on the weaker (for A) or higher (for B and C) known values in our sample of extant endotherms. A, Resting metabolic rate (RMR) inferences using a model comprising phylogeny and relative primary osteon area (RPOA). B, Red blood cell (RBC) width inferences using a model comprising phylogeny and minimal caliber (can_{min}). C, RBC area inferences using a model comprising phylogeny and can_{min}.

logarithm for RMR and natural logarithm +1 for RPOA, as it contains null values. It was not necessary to transform the data of the two other analyses, as results of Shapiro-Wilk tests were not significant ($p = 0.9577$ for RBC_w analysis; $p = 0.6624$ for RBC_a analysis).

As data for RMR inferences were log transformed, the confidence interval is asymmetric after de-transformation. We found very low values of RMR for both taxa (†$Dyrosaurus$ = [0.23; 0.14–0.36] ml(O_2) h^{-1} $g^{-0.67}$; †$Goniopholis$ = [0.21; 0.14–0.30] ml(O_2) h^{-1} $g^{-0.67}$), close to what we observed in $Crocodylus$ (0.331 ml(O_2) h^{-1} $g^{-0.67}$) and in $Caiman$ (0.12 ml(O_2) h^{-1} $g^{-0.67}$). These values and the corresponding confidence intervals are lower than the minimal known value for an endotherm (cf. $Microcebus$, RMR = 1.526 ml(O_2) h^{-1} $g^{-0.67}$) and are close to the maximal known value for an ectotherm (cf. $Crocodylus$, RMR = 0.331 ml(O_2) h^{-1} $g^{-0.67}$; Fig. 5A). Hence, we can conclude both †$Dyrosaurus$ and †$Goniopholis$ had an RMR close to their extant relatives, within the range of ectotherms.

A similar situation is observed for RBC_a, with values inferred for both taxa similar to those observed in extant relatives ($Alligator$ = 159.4 μm^2; †$Dyrosaurus$ = 165.94 ± 25.68 μm^2; †$Goniopholis$ = 132.35 ± 18.55 μm^2) and superior to the maximum known value for endotherms (cf. $Columba$ = 69.5 μm^2) and the minimal known value for ectotherms (cf. $Varanus$ $exanthematicus$ = 99.4 μm^2; Fig. 5C). For the RBC_w inference, the situation is similar for †$Dyrosaurus$ (RBC width = 11.85 ± 1.75 μm), but the confidence interval of †$Goniopholis$ (RBC width = 8.42 ± 1.17 μm) includes the maximal known values of endotherms (cf. $Neovison$ = 7.8 μm). Both their central values are still close to the $Alligator$ value (RBC_w = 10 μm; Fig. 5B). Thus we can conclude that both taxa displayed RBC_a in the range of extant ectotherms and †$Dyrosaurus$ had RBC_w in the range of extant

ectotherms too. However, considering that the confidence interval of the inference for †$Goniopholis$ overlaps the values observed in ectotherms and endotherms, no conclusion can be outlined for this taxon using this model.

Isotopic Geochemistry

$Tiupampa$.—Oxygen isotope composition of phosphates from Tiupampa vertebrates are presented in Table 3, along with the estimated water $\delta^{18}O_{aw}$ values calculated by using equations (3) to (5). Mammals point to a source of drinking water with an average $\delta^{18}O_w$ value of −5.4 ± 0.4‰ and the turtle †$Roxochelys$ to a less negative value of −2.1‰, indicating at least two distinct sources of drinking water. Using these $\delta^{18}O_{aw}$, we inferred the possible T_b of Dyrosauridae using equation (2), which is reported in Table 4. T_b estimates using †$Alcidedorbignya$ $inopinata$'s $\delta^{18}O_{aw}$ as water sources are too low for crocodylomorphs to be realistic (10°C–23°C; Table 4; Fig. 6A). However, T_b estimates using †$Roxochelys$'s $\delta^{18}O_w$ as water sources range from 25°C to 38°C and appear more coherent (Table 4; Fig. 6A). This range of body temperatures covers that of modern crocodilians and is compatible with an ecto-poikilothermic thermometabolism for dyrosaurids.

$Cherves-de-Cognac$.—Published isotopic values from Pouech et al. (2014) include those of †$Goniopholis$ along with those of the theropod cf. †$Nuthetes$, the turtles †$Pleurosternon$ and †$Tretosternon$, as well as the mammals †$Pinheirodon$ and some indeterminate Spalacotheriidae and Dryolestidae (Table 3). Using equations (3) to (5), local water $\delta^{18}O_{aw}$ values have been calculated and two major sources have been identified: the first one, calculated from both turtles and theropods, ranges from 1.0 ± 1.0‰ to 1.2 ± 0.3‰; and the second one, calculated from mammals, has an average value of −3.3 ± 1.3‰ (Table 4). T_b estimates

TABLE 3. Oxygen isotope composition of phosphate ($\delta^{18}O_p$) from vertebrates of Tiupampa and isotopic values extracted from Pouech et al. (2014) for Cherves-de-Cognac are reported along with calculated oxygen isotope composition of their drinking water ($\delta^{18}O_w$) using phosphate water fractionation equations (3) to (5) (see text).

Taxa	$\delta^{18}O_p$ (‰VSMOW)	$\delta^{18}O_w$ (‰VSMOW)	Source
Paleocene of Tiupampa (Bolivia)			
Dyrosauridae indet.	20.4	—	This study
	19.9	—	This study
	17.5	—	This study
	18.3	—	This study
†*Alcidedorbygnia inopinata*	18.5	−5.8	This study
	18.7	−5.6	This study
	19.2	−5.0	This study
	19.3	−4.9	This study
†*Roxochelys* sp.	19.2	−2.1	This study
Berriasian of Cherves-de-Cognac (France)			
†*Goniopholis* sp.	22.1	—	Pouech et al. 2014
	21.8	—	Pouech et al. 2014
	21.3	—	Pouech et al. 2014
†*Pleurosternon* sp.	21.6	0.3	Pouech et al. 2014
†*Tretosternon* sp.	23.0	1.7	Pouech et al. 2014
Theropoda cf. †*Nuthetes*	22.5	1.0	Pouech et al. 2014
	23.0	1.5	Pouech et al. 2014
	22.6	1.1	Pouech et al. 2014
†*Pinheirodon pygmaeus*	22.1	−1.8	Pouech et al. 2014
Spalacotheriidae	20.1	−4.0	Pouech et al. 2014
Dryolestidae	20.2	−3.9	Pouech et al. 2014

using mammals' $\delta^{18}O_{aw}$ values as water sources are too low for crocodylomorphs to be realistic (12°C–16°C). However, using turtles' and theropods' $\delta^{18}O_{aw}$ values as water sources, T_b estimates, which range from 31°C to 36°C (Table 4; Fig. 6B), cover that of modern crocodilians and are compatible with an ecto-poikilothermic thermometabolism for †*Goniopholis*.

Discussion

Histology

Qualitative and quantitative histological analyses lead to the same conclusion: †*Goniopholis* and †*Dyrosaurus* possessed a thermometabolic regime similar to that of extant crocodilians. Their bone microstructure and histological organization depict a first burst of growth, early during the post-hatching ontogeny, followed by a succession of periods of relatively high and low BGR, as suggested by the lamellar-zonal organization. However, this is not definitive evidence to infer a low metabolic rate, as some endotherms display typical ectothermic bones (Reid 1984). It is worth considering that Legendre et al. (2016) inferred an

endothermic metabolism for †*Calyptosuchus* (Aetosauria) and †*Postosuchus* (Rauisuchidae), based on their inferred RMR values, but their bone organization is lamellar-zonal too (de Ricqlès et al. 2003), similar to those observed in †*Goniopholis* and †*Dyrosaurus*. Therefore, qualitative histology seems insufficient to infer their metabolism.

The inference of RMR with quantitative histology supports the hypothesis of two ectothermic taxa. We preferred to use a model comprising a histological variable, as both models (phylogeny only and phylogeny combined with bone histology) are similar in terms of AICc and R^2 parameters. Moreover, in previous studies, RPOA was preferred to the model without it (Fleischle et al. 2018; Faure-Brac and Cubo 2020). Regardless, the choice of one model over other with equivalent scores does not matter, as it will only slightly modify the inferred variables. We inferred a low RMR value despite the fact that RPOA was quantified in layers displaying the highest BGR, hence associated to the highest RMR. The RBC_a and RBC_w inferences point in the same direction. For both variables, values inferred for †*Dyrosaurus* fall within the range of those

TABLE 4. Calculated dyrosaurids and †*Goniopholis* body temperatures (T_b) using water δ18Ow values derived from associated turtles, mammals, and theropods and by applying equation 2 (see text).

Taxon	Locality	δ18Op (‰VSMOW) min	δ18Op (‰VSMOW) max	δ18Ow (‰VSMOW) from turtles	Crocodylomorph T_b range (°C)	δ18Ow (‰VSMOW) from mammals	Crocodylomorph T_b range (°C)	δ18Ow (‰VSMOW) from theropods	Crocodylomorph T_b range (°C)
Dyrosauridae indet.	Tiupampa	17.5	20.4	−2.1 ± 0.0	25–38	−5.4 ± 0.4	10–23	—	—
†*Goniopholis* sp.	Cherves-de-Cognac	21.3	22.1	1.0 ± 1.0	31–35	−3.3 ± 1.3	12–16	1.2 ± 0.3	32–36

measured in extant ectotherms (characterized by the presence of large RBCs). A similar result is observed for †*Goniopholis*, but only for RBC$_a$. Inferred values of RBC$_w$ for †*Goniopholis* are inconclusive, because the associated 95% confidence interval overlaps values measured in extant ectotherms and extant endotherms. The inference of RBC$_w$ is the least conclusive of our analyses, as the model is the less supported ($R^2 = 0.828$) and should be viewed with more caution than the two others. As high values of RBC$_a$ and RBC$_w$ are causally linked to low metabolic rates (Holland and Forster 1966; Huttenlocker and Farmer 2017; Cubo et al. 2020), our inferences of RBC dimensions are congruent with our RMR estimations. To achieve a higher metabolic rate and then endothermy, a higher amount of produced energy is required, which demands increased oxygen uptake to sustain the energetic production. The reduction of the size of RBCs is a powerful solution: smaller RBCs are more efficient supplying in oxygen (Snyder and Sheafor 1999; Soslau 2020).

All histological analyses draw the same general picture suggesting that both taxa probably shared a low RMR, typical of what we observed in their extant relatives. Therefore, on the basis of our data, we conclude that both †*Dyrosaurus* and †*Goniopholis* were ectothermic vertebrates.

Isotopic Geochemistry

The new isotopic data obtained from the Tiupampa fauna and a review of the Cherves-de-Cognac fauna data allowed us to estimate the T_b for both our taxa, using the available relationships linking T_b to δ18O$_p$ and δ18O$_{bw}$. Extant crocodiles are polyphiodonts, that is, their teeth are continually replaced during a large part of their life (Poole 1961). Therefore, we have access to a single brief record of T_b in the life of the specimen. As each tooth can be replaced up to 45 times in the lifetime of an extant crocodilian (Poole 1961), their formation records only a short moment of the animal's life, but it is large enough to provide the entire range of thermal behavior of a typical semi-aquatic organism, such as extant crocodilians. †*Goniopholis* would be expected to follow that pattern if it was ectothermic. In contrast, dyrosaurids were marine in their great majority
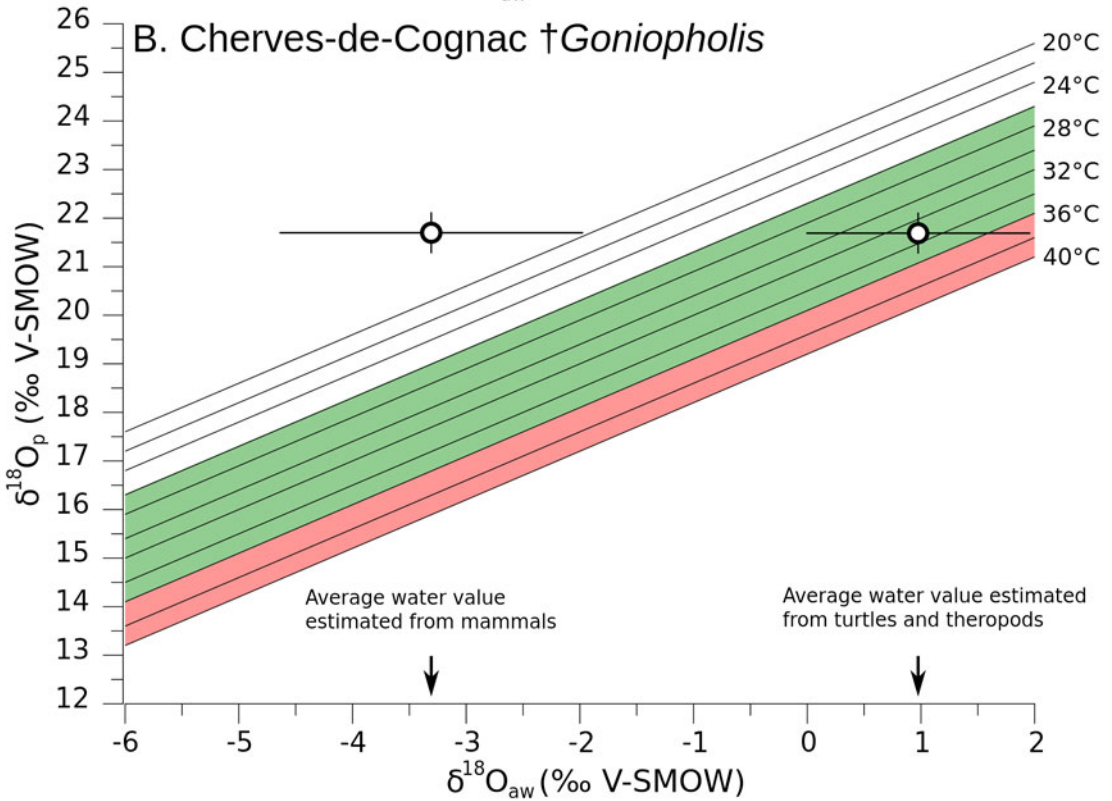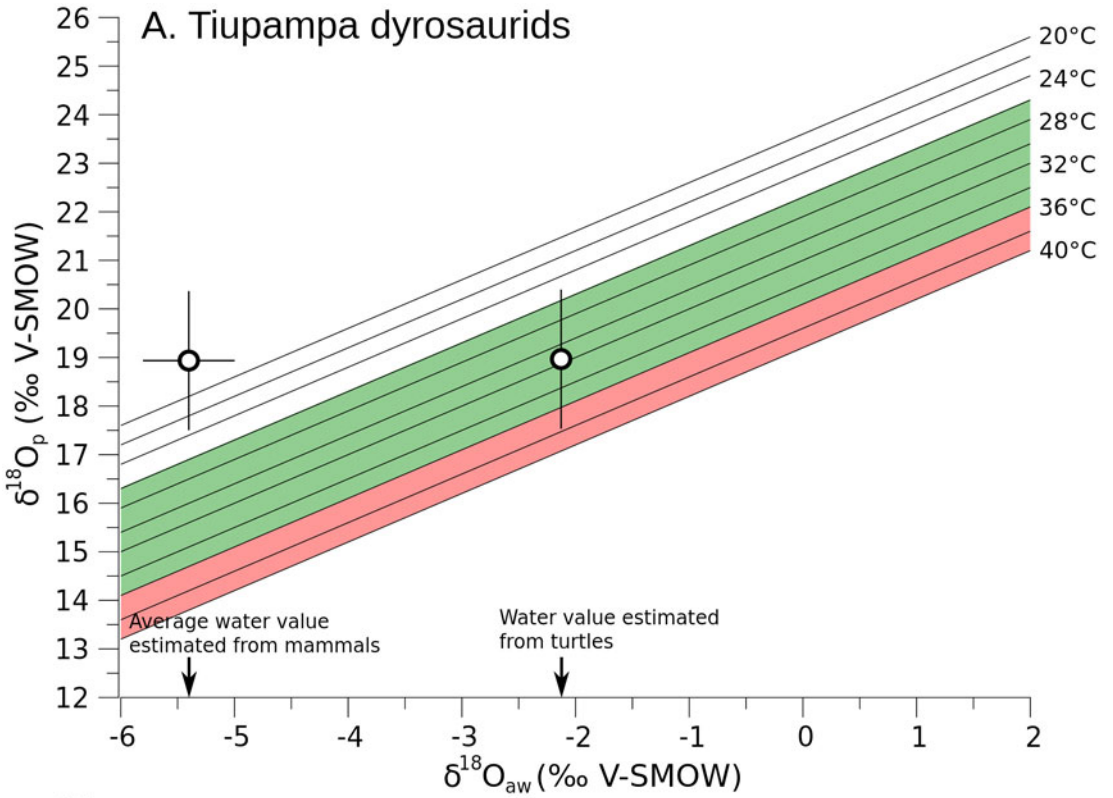
A. Tiupampa dyrosaurids

B. Cherves-de-Cognac †*Goniopholis*

FIGURE 6. Dyrosaurid (A) and †*Goniopholis* (B) $\delta^{18}O_p$ values are plotted against their possible ambient water $\delta^{18}O_{aw}$ values within a frame showing expected vertebrate $\delta^{18}O_p$–$\delta^{18}O_{aw}$ plot for a range of body temperatures (black lines). The green area represents expected body temperature (T_b) range for modern crocodilians, and the red area represents the expected T_b range for modern endotherms.

(Wilberg et al. 2019). Although polyphiodonts, their living environment was much more thermally buffered because of their aquatic ecology. An ectothermic dyrosaurid should then have recorded an aquatic environment close to marine water; however, the estimated negative $\delta^{18}O$ values indicate that dyrosaurids from Tiupampa most likely lived in a ^{18}O-depleted freshwater environment such as an estuary or a river. Two dyrosaurid species have been documented so far, which are of similar geological age (the Maria Farinha Formation, Brazil): †*Guarinisuchus munizi* and †*Hyposaurus derbianus*, both known as marine species (Wilberg et al. 2019). Therefore, our studied dyrosaurids were either marine species living at the mouth of an estuary, being in this case similar to the species from the Maria Farinha Formation, or we sampled an unknown freshwater species.

Using water $\delta^{18}O_{aw}$ values estimated from coexisting turtles and from theropod dinosaurs at Cherves-de-Cognac, calculated dyrosaurid and †*Goniopholis* T_b values fall in the "preferred" temperature range of extant crocodilian body temperature (26°C–36°C). However, the calculated T_b values for both dyrosaurids and †*Goniopholis* are unrealistically low when using mammal-derived $\delta^{18}O_w$ values. It is noteworthy that Pouech et al. (2014) considered it improbable that †*Goniopholis* shared the same environment as mammals, as the latter would be expected to live in forests and the former in an estuary-like environment, and similar reasoning could be proposed for the small pantodont mammals †*Alcidedorbignya*, which have been considered by de Muizon et al. (2015) to be a terrestrial animal with possible scansorial habits, compatible with a forest habitat. Therefore, the ambient waters ingested by mammals in both cases were most likely not the waters inhabited by dyrosaurids and †*Goniopolis*. Once again, we consider both Dyrosauridae and †*Goniopholis* as ectothermic using this proxy.

Integrative Approach

RMR and RBC dimensions inferred for †*Dyrosaurus* and †*Goniopholis* using quantitative histology fall in the range of variations measured in extant ectotherms. Moreover, oxygen isotopes of apatite phosphate suggest a range of body temperatures compatible with that of extant crocodilians. Despite the specific limits of both approaches, results converge, suggesting an ectothermic status for the two vertebrate taxa studied here, even though such interpretations must be made with caution.

Isotopic geochemistry only provides a rough estimate of T_b and depends on the proper estimation of drinking water $\delta^{18}O_w$ value based on coexisting vertebrates' $\delta^{18}O_p$ values. Moreover, T_b is only a product of thermometabolism and not entirely driven by it. A high T_b is necessary but not sufficient in itself to infer endothermy. Gigantothermy could be a possibility to explain high body temperatures, but it still has to be proven that an endotherm-like T_b can be reached this way. Known extant cases of gigantothermy roughly attain ~30°C (Paladino et al. 1990). For extinct cases, it was theorized that large dinosaurs could achieve homoiothermy with a T_b of ~31°C (Seebacher et al. 1999).

Quantitative histology allows inferring metabolic rate using phylogenetic comparative methods. It possesses its known issues, as it cannot robustly detect ectothermy, because bone structure produced by an ectothermic animal can easily be formed by endothermic ones as well. Moreover, it cannot detect particular cases such as putative gigantothermy (high T_b but low RMR). In addition, we cannot be fully certain that a high RMR always indicates endothermy. As mentioned before, the link between these variables is correlational.

Conclusion

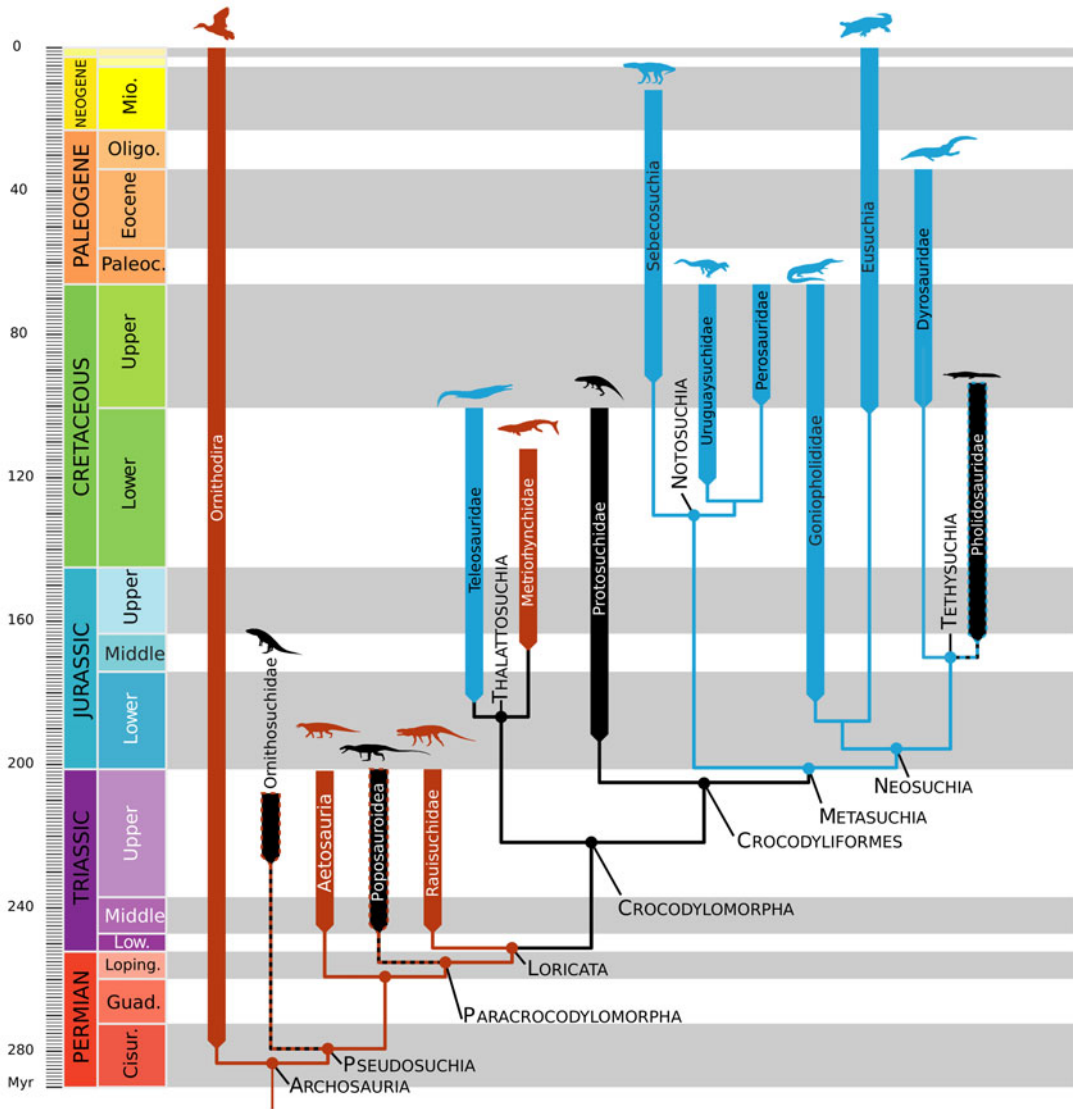This study, along with those published by Cubo et al. (2020), Legendre et al. (2016), and

FIGURE 7. Summary of the distribution of thermometabolism across Archosauria. The phylogeny used is a handmade combination of both trees presented in Puértolas-Pascual et al. (2020) and Nesbitt (2011). Red indicates an inferred or known endothermic taxon. Blue indicates an inferred or known ectothermic taxon. Black indicates unknown status. Black surrounded by dotted colored lines indicates a putative endothermic/ectothermic status depending on the color used. Shapes were taken from phylopic.org.

Séon et al. (2020), explores the evolution of thermometabolism among the pseudosuchians and, more especially, the loss(es) of their ancestral endothermy (Seymour et al. 2004). A hypothesis suggesting a loss linked to the acquisition of a semiaquatic lifestyle and ambush predation was proposed (Seymour et al. 2004). However, hypothesizing that Pholidosauridae were ectotherms as Dyrosauridae (on the basis of their close phylogenetic relationship and shared similar lifestyles, morphologies, and predation type) would imply a unique loss of endothermy at the node Metasuchia as a parsimonious explanation (Fig. 7) or even earlier at the node Crocodyliformes or Crocodylomorpha. Therefore, ectothermy may be ancestral for all metasuchians. Wilberg et al. (2019) stated that a terrestrial lifestyle is ancestral among Crocodylomorpha and Metasuchia and that the acquisition of a

semiaquatic lifestyle and ambush predation is a specificity of Neosuchia. Seymour et al.'s (2004) hypothesis about an ancestral endothermic state for archosaurs is thus corroborated, but their hypothesis about the loss of endothermy linked to the acquisition of a semiaquatic lifestyle and ambush predation is rejected, because terrestrial Notosuchia are inferred to be ectotherms (Cubo et al. 2020) and Metasuchia are inferred to be ancestrally terrestrial. However, the ambiguous status of *Calsoyasuchus* could lead to a review of this interpretation if it considered to be amphibious (Wilberg et al. 2019: fig. 6).

Legendre et al. (2016) inferred endothermic-like RMR for †*Postosuchus* (Rauisuchidae) and †*Calyptosuchus* (Aetosauria), both external to the clade Crocodylomorpha. Séon et al. (2020) proposed ectothermic Teleosauridae and endothermic–heterothermic Metriorhynchidae, with a doubt concerning the ancestral status of thalattosuchians. The last missing pieces are the status of Protosuchidae and some stem species, like †*Hsisosuchus*, which should bring the final necessary data to constrain the reversion(s) of thermometabolic condition in Pseudosuchia (Fig. 7).

We suggest that combined bone paleohistology and stable isotope geochemistry should be used whenever possible to contrast inferences and produce more robust interpretations.

Acknowledgments

Data Availability Statement

Data available from the Dryad Digital Repository: https://doi.org/10.5061/dryad.4xgxd259v.

Literature Cited

Amiot, R., C. Lécuyer, E. Buffetaut, F. Fluteau, S. Legendre, and F. Martineau. 2004. Latitudinal temperature gradient during the Cretaceous Upper Campanian–Middle Maastrichtian: δ18O record of continental vertebrates. Earth and Planetary Science Letters 226:255–272.

Amiot, R., C. Lécuyer, E. Buffetaut, G. Escarguel, F. Fluteau, and F. Martineau. 2006. Oxygen isotopes from biogenic apatites suggest widespread endothermy in Cretaceous dinosaurs. Earth and Planetary Science Letters 246:41–54.

Amiot, R., C. Lécuyer, G. Escarguel, J.-P. Billon-Bruyat, E. Buffetaut, C. Langlois, S. Martin, F. Martineau, and J.-M. Mazin. 2007. Oxygen isotope fractionation between crocodilian phosphate and water. Palaeogeography, Palaeoclimatology, Palaeoecology 243:412–420.

Amiot, R., X. Wang, Z. Zhou, X. Wang, C. Lécuyer, E. Buffetaut, F. Fluteau, Z. Ding, N. Kusuhashi, J. Mo, M. Philippe, V. Suteethorn, Y. Wang, and X. Xu. 2015. Environment and ecology of East Asian dinosaurs during the Early Cretaceous inferred from stable oxygen and carbon isotopes in apatite. Journal of Asian Earth Sciences 98:358–370.

Amprino, R. 1947. La structure du tissu osseux envisagée comme expression de différences dans la vitesse de l'accroissement. Archives de Biologie 58:315–330.

Barrick, R. E., A. G. Fischer, and W. J. Showers. 1999. Oxygen isotopes from turtle bone; applications for terrestrial paleoclimates? Palaios 14:186–191.

Bennett, A. F., and J. A. Ruben. 1979. Endothermy and activity in vertebrates. Science 206:649–654.

Bernard, A., C. Lécuyer, P. Vincent, R. Amiot, N. Bardet, E. Buffetaut, G. Cuny, F. Fourel, F. Martineau, J.-M. Mazin, and A. Prieur. 2010. Regulation of body temperature by some Mesozoic marine reptiles. Science 328:1379–1382.

Bromage, T. G., H. M. Goldman, S. C. McFarlin, J. Warshaw, A. Boyde, and C. M. Riggs. 2003. Circularly polarized light standards for investigations of collagen fiber orientation in bone. Anatomical Record B 274B:157–168.

Clarke, A., and H.-O. Pörtner. 2010. Temperature, metabolic power and the evolution of endothermy. Biological Reviews 85:703–727.

Cubo, J., and N.-E. Jalil. 2019. Bone histology of *Azendohsaurus laaroussii*: implications for the evolution of thermometabolism in Archosauromorpha. Paleobiology 45:317–330.

Cubo, J., N. L. Roy, C. Martinez-Maza, and L. Montes. 2012. Paleohistological estimation of bone growth rate in extinct archosaurs. Paleobiology 38:335–349.

Cubo, J., M. Hui, F. Clarac, and A. Quilhac. 2017. Static osteogenesis does not precede dynamic osteogenesis in periosteal ossification of Pleurodeles (Caudata, Amphibia) and Pogona (Squamata, Lepidosauria). Journal of Morphology 278:621–628.

Cubo, J., M. V. A. Sena, P. Aubier, G. Houee, P. Claisse, M. G. Faure-Brac, R. Allain, R. C. L. P. Andrade, J. M. Sayão, and G. R. Oliveira. 2020. Were Notosuchia (Pseudosuchia: Crocodylomorpha) warm-blooded? A palaeohistological analysis suggests ectothermy. Biological Journal of the Linnean Society 131:154–162.

D'Angela, D., and A. Longinelli. 1990. Oxygen isotopes in living mammal's bone phosphate: further results. Chemical Geology: Isotope Geoscience 86:75–82.

Farmer, C. G. 2015. Similarity of crocodilian and avian lungs indicates unidirectional flow is ancestral for archosaurs. Integrative and Comparative Biology 55:962–971.

Farmer, C. G., and K. Sanders. 2010. Unidirectional airflow in the lungs of alligators. Science 327:338–340.

Faure-Brac, M. G., and J. Cubo. 2020. Were the synapsids primitively endotherms? A palaeohistological approach using phylogenetic eigenvector maps. Philosophical Transactions of the Royal Society of London B 375:20190138.

Faure-Brac, M. G., F. Pelissier, and J. Cubo. 2019. The influence of plane of section on the identification of bone tissue types in amniotes with implications for paleophysiological inferences. Journal of Morphology 280:1282–1291.

Fleischle, C. V., T. Wintrich, and P. M. Sander. 2018. Quantitative histological models suggest endothermy in plesiosaurs. PeerJ 6: e4955.

Florides, G. A., S. A. Kalogirou, S. A. Tassou, and L. Wrobel. 2001. Natural environment and thermal behaviour of *Dimetrodon limbatus*. Journal of Thermal Biology 26:15–20.

Francillon-Vieillot, H., V. de Buffrénil, J. Castanet, J. Géraudie, F. J. Meunier, J.-Y. Sire, L. Zylberberg, and A. J. de Ricqlès. 1990. Microstructure and mineralization of vertebrate skeletal tissues. Pp. 471–530 *in* J. G. Carter, ed. Skeletal biomineralization: patterns, processes and evolutionary trends, Vol. 1. VanNostrand Reinhold, New York.

Gonfiantini, R., W. Stichler, and K. Rozanski. 1995. Standards and intercomparison materials distributed by the International Atomic Energy Agency for stable isotope measurements. IAEA, Vienna.

Guénard, G., P. Legendre, and P. Peres-Neto. 2013. Phylogenetic eigenvector maps: a framework to model and predict species traits. Methods in Ecology and Evolution 4:1120–1131.

Holland, R. a. B., and R. E. Forster. 1966. The effect of size of red cells on the kinetics of their oxygen uptake. Journal of General Physiology 49:727–742.

Huttenlocker, A. K., and C. G. Farmer. 2017. Bone microvasculature tracks red blood cell size diminution in Triassic mammal and dinosaur forerunners. Current Biology 27:48–54.

Janke, A., and U. Arnason. 1997. The complete mitochondrial genome of *Alligator mississippiensis* and the separation between recent Archosauria (birds and crocodiles). Molecular Biology and Evolution 14:1266–1272.

Janke, A., D. Erpenbeck, M. Nilsson, and U. Arnason. 2001. The mitochondrial genomes of the iguana (*Iguana iguana*) and the caiman (*Caiman crocodylus*): implications for amniote phylogeny. Proceedings of the Royal Society of London B 268:623–631.

Ji, Q., Z.-X. Luo, C.-X. Yuan, and A. R. Tabrum. 2006. A swimming mammaliaform from the middle Jurassic and ecomorphological diversification of early mammals. Science 311:1123–1127.

Kohn, M. J. 1996. Predicting animal δ^{18}O. Accounting for diet and physiological adaptation. Geochimica et Cosmochimica Acta 60:4811–4829.

Kolodny, Y., B. Luz, and O. Navon. 1983. Oxygen isotope variations in phosphate of biogenic apatites, I. Fish bone apatite rechecking the rules of the game. Earth and Planetary Science Letters 64:398–404.

Lamm, E.-T. 2013. Preparation and sectioning of specimens. Pp. 55–160 *in* K. Padian and E.-T. Lamm, eds. Bone histology of fossil tetrapods: advancing methods, analysis, and interpretation. University of California Press, Berkeley.

Langlois, C., L. Simon, and C. Lécuyer. 2003. Box-modeling of bone and tooth phosphate oxygen isotope compositions as a function of environmental and physiological parameters. Isotopes in Environmental and Health Studies 39:259–272.

Lécuyer, C., P. Grandjean, J. R. O'Neil, H. Cappetta, and F. Martineau. 1993. Thermal excursions in the ocean at the Cretaceous–Tertiary boundary (northern Morocco): δ^{18}O record of phosphatic fish debris. Palaeogeography, Palaeoclimatology, Palaeoecology 105:235–243.

Lécuyer, C., R. Amiot, A. Touzeau, and J. Trotter. 2013. Calibration of the phosphate δ^{18}O thermometer with carbonate–water oxygen isotope fractionation equations. Chemical Geology 347:217–226.

Legendre, L. J., G. Guénard, J. Botha-Brink, and J. Cubo. 2016. Palaeohistological evidence for ancestral high metabolic rate in archosaurs. Systematic Biology 65:989–996.

Longinelli, A. 1984. Oxygen isotopes in mammal bone phosphate: a new tool for paleohydrological and paleoclimatological research? Geochimica et Cosmochimica Acta 48:385–390.

Luz, B., Y. Kolodny, and M. Horowitz. 1984. Fractionation of oxygen isotopes between mammalian bone-phosphate and environmental drinking water. Geochimica et Cosmochimica Acta 48:1689–1693.

Markwick, P. J. 1998. Fossil crocodilians as indicators of Late Cretaceous and Cenozoic climates: implications for using palaeontological data in reconstructing palaeoclimate. Palaeogeography, Palaeoclimatology, Palaeoecology 137:205–271.

Marotti, G. 2010. Static and dynamic osteogenesis. Italian Journal of Anatomy and Embryology 115:123–126.

McNab, B. K. 1978. The evolution of endothermy in the phylogeny of mammals. American Naturalist 112:1–21.

Montes, L., N. Le Roy, M. Perret, V. de Buffrénil, J. Castanet, and J. Cubo. 2007. Relationships between bone growth rate, body mass and resting metabolic rate in growing amniotes: a phylogenetic approach. Biological Journal of the Linnean Society 92:63–76.

Montes, L., J. Castanet, and J. Cubo. 2010. Relationship between bone growth rate and bone tissue organization in amniotes: first test of Amprino's rule in a phylogenetic context. Animal Biology 60:25–41.

Muizon, C. de, and L. G. Marshall. 1992. *Alcidedorbignya inopinata* (Mammalia: Pantodonta) from the Early Paleocene of Bolivia: phylogenetic and paleobiogeographic implications. Journal of Paleontology 66:499–520.

Muizon, C. de, G. Billet, C. Argot, S. Ladevèze, and F. Goussard. 2015. *Alcidedorbignya inopinata*, a basal pantodont (Placentalia, Mammalia) from the early Palaeocene of Bolivia: anatomy, phylogeny and palaeobiology. Geodiversitas 37:397–634.

Nesbitt, S. J. 2011. The early evolution of archosaurs: relationships and the origin of major clades. Bulletin of the American Museum of Natural History 2011:1–292.

Olivier, C., A. Houssaye, N.-E. Jalil, and J. Cubo. 2017. First palaeohistological inference of resting metabolic rate in an extinct synapsid, *Moghreberia nmachouensis* (Therapsida: Anomodontia). Biological Journal of the Linnean Society 121:409–419.

Owen, R. 1879. Monograph on the fossil Reptilia of the Wealden and Purbeck Formations. Supplement no. IX; pp. 1–19; plates I–IV. Crocodilia (*Goniopholis*, *Brachydectes*, *Nannosuchus*, *Theriosuchus*, and *Nuthetes*). Issued in the volume for the year 1879. Monographs of the Palaeontographical Society 33:1–19.

Padian, K., J. R. Horner, and A. J. de Ricqlès. 2004. Growth in small dinosaurs and pterosaurs: the evolution of archosaurian growth strategies. Journal of Vertebrate Paleontology 24:555–571.

Paladino, F. V., M. P. O'Connor, and J. R. Spotila. 1990. Metabolism of leatherback turtles, gigantothermy, and thermoregulation of dinosaurs. Nature 344:858–860.

Pomel, A. 1894. Sur le *Dyrosaurus thevestensis*. Comptes Rendus de l'Académie des Sciences 118:1396.

Poole, D. F. G. 1961. Notes on tooth replacement in the Nile crocodile *Crocodilus niloticus*. Proceedings of the Zoological Society of London 136:131–140.

Pouech, J., R. Amiot, C. Lécuyer, J.-M. Mazin, F. Martineau, and F. Fourel. 2014. Oxygen isotope composition of vertebrate phosphates from Cherves-de-Cognac (Berriasian, France): environmental and ecological significance. Palaeogeography, Palaeoclimatology, Palaeoecology 410:290–299.

Price, L. I. 1953. Os Quelônios da Formação Bauru, Cretáceo terrestre do Brasil meridional. Boletim do Departamento Nacional da Produção Mineral/Divisão de Geologia e Mineralogia, Rio de Janeiro 147:1–34.

Prondvai, E., K. H. W. Stein, A. de Ricqlès, and J. Cubo. 2014. Development-based revision of bone tissue classification: the importance of semantics for science. Biological Journal of the Linnean Society 112:799–816.

Puértolas-Pascual, E., M. T. Young, and C. A. Brochu. 2020. Introducing the first European symposium on the evolution of Crocodylomorpha. Zoological Journal of the Linnean Society 189:419–427.

Rasband, W. S. 1997. ImageJ. National Institutes of Health, Bethesda, Md.

R Development Core Team. 2008. R: a language and environment for statistical computing. R Foundation for Statistical Computing, Vienna, Austria.

Reid, R. E. H. 1984. Primary bone and dinosaurian physiology. Geological Magazine 121:589–598.

Rey, K., R. Amiot, F. Fourel, F. Abdala, F. Fluteau, N.-E. Jalil, J. Liu, B. S. Rubidge, R. M. Smith, J. S. Steyer, P. A. Viglietti, X. Wang, and C. Lécuyer. 2017. Oxygen isotopes suggest elevated thermometabolism within multiple Permo-Triassic therapsid clades. eLife 6:e28589.

Ricqlès, A. J. de. 1974. Evolution of endothermy: histological evidences. Evolutionary Theory 1:51–80.

Ricqlès, A. J. de, K. Padian, and J. R. Horner. 2003. On the bone histology of some Triassic pseudosuchian archosaurs and related taxa. Annales de Paléontologie 89:67–101.

Rowland, L. A., N. C. Bal, and M. Periasamy. 2015. The role of skeletal-muscle-based thermogenic mechanisms in vertebrate endothermy. Biological Reviews 90:1279–1297.

Ruben, J. A. 1995. The evolution of endothermy in mammals and birds: from physiology to fossils. Annual Review of Physiology 57:69–95.

Ruben, J. A., W. J. Hillenius, T. S. Kemp, and D. E. Quick. 2012. The evolution of mammalian endothermy. Pp. 273–286 in A. Chinsamy-Turan, ed. Forerunners of mammals: radiation, histology, biology. Indiana University Press, Bloomington.

Sanders, R. K., and C. G. Farmer. 2012. The pulmonary anatomy of Alligator mississippiensis and its similarity to the avian respiratory system. Anatomical Record 295:699–714.

Seebacher, F., G. C. Grigg, and L. A. Beard. 1999. Behavioural thermoregulation in crocodiles. Journal of Experimental Biology 202:77–86.

Séon, N., R. Amiot, J. E. Martin, M. T. Young, H. Middleton, F. Fourel, L. Picot, X. Valentin, and C. Lécuyer. 2020. Thermophysiologies of Jurassic marine crocodylomorphs inferred from the oxygen isotope composition of their tooth apatite. Philosophical Transactions of the Royal Society of London B 375:20190139.

Seymour, R. S. 2013. Maximal aerobic and anaerobic power generation in large crocodiles versus mammals: implications for dinosaur gigantothermy. PLoS ONE 8:10.

Seymour, R. S. 2016. Cardiovascular physiology of dinosaurs. Physiology 31:430–441.

Seymour, R. S., C. L. Bennett-Stamper, S. D. Johnston, D. R. Carrier, and G. C. Grigg. 2004. Evidence for endothermic ancestors of crocodiles at the stem of archosaur evolution. Physiological and Biochemical Zoology 77:1051–1067.

Seymour, R. S., C. M. Gienger, M. L. Brien, C. R. Tracy, S. Charlie Manolis, G. J. W. Webb, and K. A. Christian. 2013. Scaling of standard metabolic rate in estuarine crocodiles Crocodylus porosus. Journal of Comparative Physiology B 183:491–500.

Snyder, G. K., and B. A. Sheafor. 1999. Red blood cells: centerpiece in the evolution of the vertebrate circulatory system. Integrative and Comparative Biology 39:189–198.

Soslau, G. 2020. The role of the red blood cell and platelet in the evolution of mammalian and avian endothermy. Journal of Experimental Zoology B 334:113–127.

Starck, J. M., and A. Chinsamy. 2002. Bone microstructure and developmental plasticity in birds and other dinosaurs. Journal of Morphology 254:232–246.

Stein, K., and E. Prondvai. 2014. Rethinking the nature of fibrolamellar bone: an integrative biological revision of sauropod plexiform bone formation. Biological Reviews 89:24–47.

Tumarkin-Deratzian, A. R. 2007. Fibrolamellar bone in wild adult Alligator mississippiensis. Journal of Herpetology 41:341–345.

Walter, I., and F. Seebacher. 2009. Endothermy in birds: underlying molecular mechanisms. Journal of Experimental Biology 212:2328–2336.

Wilberg, E. W., A. H. Turner, and C. A. Brochu. 2019. Evolutionary structure and timing of major habitat shifts in Crocodylomorpha. Scientific Reports 9:514.

Wolf, N., S. D. Newsome, M. L. Fogel, and C. M. Del Rio. 2013. The relationship between drinking water and the hydrogen and oxygen stable isotope values of tissues in Japanese quail (Cortunix japonica). The Auk 130:323–330.

Zhou, C.-F., S. Wu, T. Martin, and Z.-X. Luo. 2013. A Jurassic mammaliaform and the earliest mammalian evolutionary adaptations. Nature 500:163–167.